Spin correlations in $Zn_{1-c}Mn_cTe$ alloys

T. M. Holden, G. Dolling, and V. F. Sears
Atomic Energy of Canada Limited, Chalk River, Ontario K0J 1J0, Canada

J. K. Furdyna
Purdue University, West Lafayette, Indiana 47907

W. Giriat
Instituto Venezolano de Investigaciones Cientificas, Centro de Fisica, Caracas, Venezuela
(Received 16 April 1982)

The nature of the spin correlations in $Zn_{1-c}Mn_cTe$ alloys for three compositions has been investigated by neutron powder diffraction methods as a function of temperature T between 300 and 2 K. The correlations, weak but observable at low c and high T, intensify progressively as c increases or T decreases, but our experiments provide no clear evidence of a phase transition to a fully ordered magnetic structure. However, the appearance of broad, intense magnetic diffuse scattering peaks near positions that could be indexed as $(1,\frac{1}{2},0)$, $(1,\frac{3}{2},0)$, and $(2,\frac{1}{2},1)$ indicates a strong tendency towards the ordering of a type-III antiferromagnet. The results are analyzed in terms of a theory of magnetic scattering from magnetic ions surrounded by near-neighbor shells of correlated spins.

I. INTRODUCTION

Recently a great deal of attention has been given to mixed semiconductor crystals whose lattice is made up in part of randomly distributed substitutional magnetic ions. These materials have often been referred to as "semimagnetic" or "diluted magnetic" semiconductors. $Hg_{1-c}Mn_cTe$ and $Cd_{1-c}Mn_cTe$ are well-known examples of this class of semiconductor alloys. Initially the interest in these materials was prompted by the fact that the exchange interaction between the localized magnetic moments and the band electrons leads to electrical and optical effects which are entirely new to semiconductor physics.[1] Recent investigations have shown that the magnetic properties of these materials are of considerable interest in their own right.[2,3] For example, $Hg_{1-c}Mn_cTe$ and $Cd_{1-c}Mn_cTe$ have been reported to manifest a spin-glass transition at low temperatures when the concentration of Mn exceeds $c=0.17$.

Neutron diffraction is an extremely powerful probe for the study of the magnetic structure in such systems and has been used to determine the spin correlations between the magnetic ions in many cases [CuMn (Refs. 4–6), AuFe (Ref. 7), $Sr_{1-c}Eu_cS$ (Ref. 8), and $Al_2Mn_3O_{12}$ (Ref. 9), to name a few characteristic materials]. In this paper we describe a series of neutron diffraction experiments on a member of the group of diluted magnetic semiconductor crystals, $Zn_{1-c}Mn_cTe$. This system was chosen for study because it forms a single crystalline phase[10] up to at least $c=0.70$ and it avoids the prohibitive neutron absorption characteristic of the only other diluted magnetic semiconductor compound which is known to form single-phase alloys to such high values of c, viz., $Cd_{1-c}Mn_cTe$.

The end member of the series, MnTe, unfortunately does not exist in the zinc-blende phase. It is therefore the introduction of Zn into the lattice which appears to have the effect of stabilizing the zinc-blende structure. The magnetic structure of the related material, zinc-blende MnS, was determined[11] to be a type-III antiferromagnet. For a thorough discussion of the domains of stability of various magnetic structures on an fcc lattice, see Ref. 12.

The outline of the paper is as follows. The theoretical model used to analyze the data is described briefly in Sec. II, together with the required scattering cross sections. In Sec. III, the experimental procedures including sample preparation are described. The experimental results are presented in Sec. IV, and Sec. V is devoted to the analysis of the experiments and discussions of the magnetic structure of $Zn_{1-c}Mn_cTe$ and related materials.

II. THEORY

The differential scattering cross section for a neutron diffraction experiment with an alloy of the

type $M_cA_{1-c}B$, where there is a random substitution of magnetic atoms (M) in place of the nonmagnetic atoms (A), is given by an average over the square of the scattering amplitude,

$$\frac{d\sigma}{d\Omega}=\langle\,|\Phi|^2\rangle\,, \tag{1}$$

where, for a structure with one formula unit per unit cell,

$$\Phi=\sum_l[\eta_l(\Phi_{M,l}-\Phi_{A,l})+\Phi_{A,l}+\Phi_{B,l}]\,. \tag{2}$$

The idempotent quality η_l is unity if an M atom occupies the lth lattice site and zero otherwise. The individual scattering amplitudes are

$$\Phi_{M,l}=[-b_M+2\gamma r_e f(Q)\vec{s}\cdot\vec{S}_l^{\perp}]\exp(i\vec{Q}\cdot\vec{R}_l)\,, \tag{3}$$

$$\Phi_{A,l}=-b_A\exp(i\vec{Q}\cdot\vec{R}_l)\,, \tag{4}$$

$$\Phi_{B,l}=-b_B\exp[i\vec{Q}\cdot(\vec{R}_l+\vec{r})]\,. \tag{5}$$

In Eq. (3) b_X is the nuclear scattering length of atom X, $\vec{S}_l^{\perp}$ is the projection of the electronic spin perpendicular to the scattering vector $\vec{Q}$, $\vec{s}$ is the neutron spin, and $f(Q)$ is the magnetic form factor. The vector $\vec{R}_l$ denotes the position of the site l in the lattice and $\vec{r}$ is the basis vector connecting A and B sites. The scattering vector $\vec{Q}=\vec{k}_0-\vec{k}'$ is the difference between the incident and scattered neutron wave vectors, and γ and r_e are the neutron gyromagnetic ratio and the classical electron radius, respectively. The average in Eq. (1) has to be taken over the statistical distribution of magnetic atoms, the electron-spin direction, the neutron-spin direction, assuming the beam is unpolarized, and, for a powder sample, over all orientations of the crystal lattice with respect to the incident beam. It is assumed for the present that the nuclear incoherent scattering is absent but it is an easy matter to include it at a later stage. Upon carrying out these averages with the assumption that η_l and $\vec{S}_l^{\perp}$ are, to a good approximation, statistically independent, the expression (6) below is obtained for the differential scattering cross section,

$$\frac{d\sigma}{d\Omega}=N\left\{\frac{\pi^2}{k_0^3V_0}\sum_h\frac{M_hF_h^2\delta(2\theta-2\theta_h)\exp(-2W_h)}{\sin\theta_h\sin2\theta_h}+c(1-c)(b_A-b_M)^2+\tfrac{2}{3}S(S+1)(\gamma r_e)^2f^2(Q)[c+c^2g(Q)]\right\}. \tag{6}$$

The first term in Eq. (6) is the nuclear Bragg scattering from the site average scattering length and the second and third terms represent diffuse nuclear and magnetic scattering, respectively. Here $k_0=2\pi/\lambda$, where λ is the wavelength of the neutrons, V_0 is the unit cell volume, N is the number of unit cells in the sample, M_h is the multiplicity of the hth reflection, 2θ is the scattering angle, θ_h is the Bragg angle, c is the Mn concentration, and F_h is the unit-cell structure factor, which is given for the zinc-blende structure by

$$F_h=cb_M+(1-c)b_A+b_B\exp[i\pi(h+k+l)/2]\,, \tag{7}$$

in which h stands for the Miller indices (h,k,l). In reality the Debye-Scherrer peaks have a finite width due to experimental resolution and finite grain size so for comparison with experiment the δ function may be replaced by a Gaussian form. The crucial part of the magnetic diffuse scattering, which allows for the correlations between the spins, is

$$g(Q)=\sum_{l\neq0}[A_lj_0(QR_l)+B_lj_2(QR_l)]\,, \tag{8}$$

with

$$A_l=\frac{1}{S(S+1)}\langle\vec{S}_0\cdot\vec{S}_l\rangle\,, \tag{9}$$

and

$$B_l=\frac{1}{S(S+1)}[\langle S_{0z}S_{lz}\rangle-\tfrac{1}{2}(\langle S_{0x}S_{lx}\rangle+\langle S_{0y}S_{ly}\rangle)]\,. \tag{10}$$

The spherical Bessel functions j_0,j_2 arise from averaging over the spin directions and from the axial symmetry of the spin tensor with respect to the vectors R_l. The z axis for each value of l is the vector joining the positions of the zeroth and lth sites. If the absolute cross section is measured, it is possible to determine both S and the spin-correlation functions. For the range of Q values in the present experiment $j_2(QR_l)\approx-j_0(QR_l)$ so that, in effect, only A_l-B_l can be determined by fitting Eq. (8) to experimental results of the present accuracy. Similar expressions for the magnetic correlations in

amorphous materials have been used by Nagele *et al.*[9] It is convenient to reinterpret the parameters A_l in Eq. (8) as the sum over all sites with the same R_l, i.e., as the net correlation within a given coordination shell. The summation index runs over discrete coordination shells. In the present analysis $A_l - B_l$ was treated as a fitting parameter for each shell of neighbors so as to measure the size and range of the correlations. It is instructive and straightforward to derive A_l and B_l for each shell of neighbors on the basis of the ideal spin structure of the material, that is the type-III antiferromagnetic structure. The parameter B_l depends on the spin direction in the ideal structure.

From the magnetic diffuse scattering (MDS) we can obtain the wave-vector–dependent magnetic susceptibility via the relation[13]

$$\left.\frac{d\sigma}{d\Omega}\right|_{\mathrm{MDS}} = (\gamma r_e)^2 \frac{2kT}{g^2\mu_B^2}\chi(Q)f^2(Q) \ . \tag{11}$$

The static susceptibility per formula unit, allowing for spin correlations, is therefore given by

$$\chi(0) = \tfrac{1}{3}g^2\mu_B^2 \frac{S(S+1)}{kT} c[1+cg(0)] \ , \tag{12}$$

so that, knowing the temperature variation of $g(0)$, the temperature dependence of the susceptibility can be calculated and vice versa.

The additional contribution of the diffuse intensity from the incoherent nuclear scattering from each component, is given by

$$\frac{d\sigma}{d\Omega} = \frac{N}{4\pi}[\sigma_B^{\mathrm{inc}} + c\sigma_M^{\mathrm{inc}} + (1-c)\sigma_A^{\mathrm{inc}}] \ . \tag{13}$$

The contribution to the diffuse intensity from inelastic scattering, or thermal diffuse scattering, may be written in the incoherent approximation as

$$\frac{d\sigma}{d\Omega} = N\{b_B^2 + [cb_M + (1-c)b_A]^2\}(1-e^{-2W}) \ , \tag{14}$$

where $\exp(-2W)$ is an average Debye-Waller factor.

In addition to these contributions, the observed counts must be corrected for multiple scattering and self-shielding. Following Sears,[14] the observed counts C are related to the true cross section by

$$C = KH(k_0,k')(1+m)\frac{d\sigma}{d\Omega} \ , \tag{15}$$

where K is the instrumental normalization factor, $H(k_0,k')$ is the absorption factor ($\simeq 10\%$) which is independent of angle for our experimental arrangement, and m is the multiple-scattering correction which is $\simeq 1.6\%$ for the $Zn_{1-c}Mn_cTe$ samples.

III. EXPERIMENTAL PROCEDURE

The $Zn_{1-c}Mn_cTe$ samples for $c = 0.68$, 0.594, and 0.376 were first prepared as bulk ingots grown from the melt by the Bridgman method. The ingots were crushed and sieved so that the maximum grain size was less than 100 μm.

The experiment was carried out using the $L3$ triple-axis crystal spectrometer at the National Research Universal (NRU) reactor, Chalk River, in the diffractometer mode with the (113) planes of a squeezed germanium crystal as monochromator at a fixed takeoff angle of 48.69°, corresponding to a neutron wavelength $\lambda = 1.406$ Å ($E_0/h = 10$ Thz, $E_0 = 41.4$ meV). The crystal mosaic spread was 0.2° and the collimation before and after the sample was 0.32°. Measurements were made over a range of scattering angles from 5° to 100° to establish the coherent scattering, but better statistics were obtained at low angles where the magnetic diffuse scattering is strongest. Typical low-angle Bragg peaks had widths [full width at half maximum (FWHM)] of 0.4°. A short experiment was carried out to check that the diffuse scattering was primarily elastic (as opposed, for example, to a spin-wave contribution) and for that experiment the (113) planes of a second germanium crystal were used to determine the scattered-neutron energies.

The powder samples were packed in thin-walled aluminum cans (i.d. 7 mm, length 50 mm) and weighed to find the effective density. A typical packing fraction was about 0.6. The sample was placed in a variable temperature cryostat permitting measurements to be made between 2 and 300 K. An empty-can run in the cryostat was made in order to measure the background, which becomes appreciable at scattering angles less than 6° due to air scattering. The Bragg scattering from the Al was used to measure the instrumental widths of the powder peaks in order to extract information about the sample homogeneity from the Bragg peak widths.

With improved accuracy of the coherent and incoherent scattering cross sections[15] of the individual components of the alloy, the Bragg-peak intensities provided three pieces of information: (i) The concentration of Mn atoms in the samples. The relative intensities of the three families of peaks ($h+k+l = 4n$, $4n\pm 2$, and $4n\pm 1$ where n is an integer) are very sensitive to concentration since the

scattering lengths of zinc and manganese have opposite signs. (ii) An effective Debye-Waller factor. This in turn permits the calculation of the thermal diffuse scattering via Eq. (14). (iii) A normalization factor for each sample studied enabling us to put the observed diffuse scattering on an absolute scale. Agreement between intensity calibrations on the same sample at different temperatures was $\pm 5\%$.

The normalization factor was also measured with a cylindrical vanadium sample of known diameter and irradiated length, correcting the observed counts for self-shielding and multiple scattering (8.7%). Agreement between the two methods, with vanadium and internally, was within 5%.

IV. EXPERIMENTAL RESULTS

The diffraction pattern for $Mn_{0.594}Zn_{0.406}Te$ at 4.2 K between 5° and 75° is shown in Fig. 1. The results show the expected pattern of Bragg peaks for the zinc-blende structure, with Al powder peaks from the can superposed on a diffuse background. The principle feature of the diffuse scattering is a broad peak (much wider than the experimental resolution given by the Bragg peaks) centered on 14.5°, which may be indexed as $(1,\frac{1}{2},0)$. Two other diffuse peaks are identifiable; that near 23.3° may be indexed as $(1,\frac{3}{2},0)$ [it is partly overlaid by the adjacent (111) nuclear peak] while the other, near 30.5°, may be indexed as $(2,\frac{1}{2},1)$. Similar diffraction patterns were also observed for $Mn_{0.376}Zn_{0.624}Te$ and $Mn_{0.68}Zn_{0.32}Te$ except that for the latter sample there was evidence for small amounts of other phases ($MnTe_2$, hexagonal MnTe) in the sample.

The parameters describing the structure, Mn concentration, Debye-Waller factor, lattice parameter, and intensity scaling factor, obtained by least-squares fitting to the integrated powder diffraction intensities and angles, are collected in Table I. The table also contains estimates derived from the (220) and (422) reflections of $Mn_cZn_{1-c}Te$ of the homogeneity of the samples based on the Bragg widths. Any excess width, above the instrumental resolution, is assumed to be due to a spread of lattice parameters in the sample. The homogeneity of the two samples of lower concentration is indeed excellent by this criterion. However, there appear to be concentration fluctuations (FWHM about 10%) in the $c=0.68$ sample that may be connected with the appearance of impurity phases. For this reason our results for this concentration have qualitative rather than quantitative significance.

The temperature dependence of the diffuse scattering between 5° and 32.9° for each of the three concentrations is shown in Figs. 2–4. The results are corrected for the empty can and for air scattering at low scattering angles. In each case, the

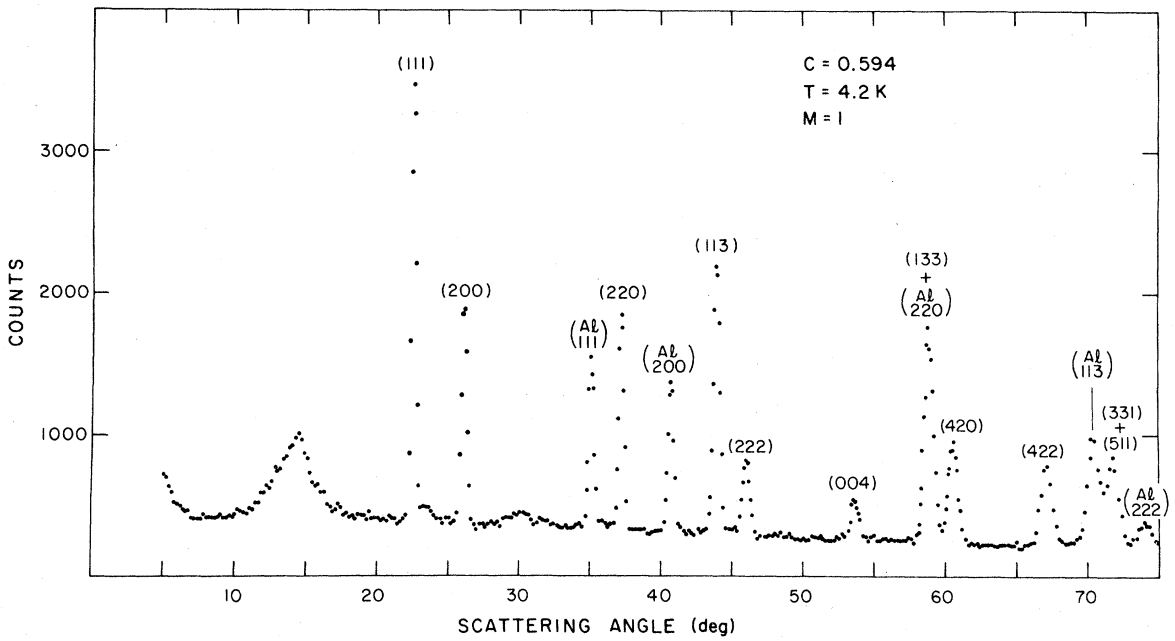

FIG. 1. Neutron diffraction pattern for $Mn_{0.594}Zn_{0.406}Te$ at 4.2 K, showing Bragg scattering from the zinc-blende structure, the aluminum sample can, and strong magnetic diffuse scattering, which peaks at 14.5°.

TABLE I. Experimental parameters for $Mn_cZn_{1-c}Te$ alloy derived from diffraction experiments. The lattice parameter is denoted by a, Δa is the rms variation of the lattice parameter derived from the width of particular Bragg reflections, and $\langle u_x^2 \rangle$ is the mean-square displacement averaged over the species in the alloy.

c (at. %)	T (K)	a ±0.001 (Å)	u_x^2 (Å^2)	Calibration factor[a] counts/ (b/sr at.)	FWHM(220)[b] (deg)	FWHM(422)[c] (deg)	Δa(220) (Å)	Δa(422) (Å)
37.6±0.3	77.6	6.176	0.0051±0.0004	452± 2	0.47±0.02	0.90±0.04	0.06 ±0.04	0.0 ±0.15
59.4±0.2	240	6.236	0.0131±0.0006	380± 4				
59.3±0.3	4	6.230	0.0047±0.0008	408± 4	0.45±0.02	0.92±0.04	0.04 ±0.05	0.03 ±0.06
68.0±0.7	300	6.263	0.0156±0.0021	382±10	0.53±0.02	0.95±0.04	0.097±0.020	0.048±0.050

[a]Monitor ($m = 1$).
[b]The instrumental width for this reflection is 0.435±0.02°.
[c]The instrumental width for this reflection is 0.903±0.04°.

dashed lines give the underlying nuclear diffuse scattering (incoherent plus thermal diffuse scattering) which accounts for the background at high angles where the magnetic form factor is negligible. As the temperature is raised the diffuse peak near 14.5° weakens, becomes broader, and shifts to lower angles. The peak is of course an indication of correlations between Mn spins which are strongest at low temperatures and decrease in strength as the temperature is raised. The width of the peak is a measure of the range of correlations between the spins. The correlations persist to high temperatures even for the $c = 0.376$ sample since the 300-K data are not well described by a Mn^{2+} magnetic form factor. The correlations also are evidently enhanced as the manganese concentration is increased. It has been assumed in this work that there is no nuclear short-range order on the (Mn,Zn) sublattice. This is, we feel, a reasonable assumption since there are no sharp features persisting at room temperature, and because the spectrum appears to evolve quite smoothly as the temperature increases. One might expect little chemical short-range ordering since Mn^{2+} and Zn^{2+} ions have rather similar ionic sizes and the transition-metal ions are in any event separated by the tellurium ions.

In addition to the principal magnetic peak, the two weaker short-range magnetic order peaks near $2\theta = 23.3°$ and 30.5° in the low-temperature data become sharper as the Mn concentration is increased from $c = 0.594$ to 0.676. The analysis shows that it is possible to understand their behavior in the growth of correlations to several shells of neighbors.

The question of long-range magnetic order, i.e., a phase transition to the ordered antiferromagnetic state, can be definitively settled for $c = 0.594$, since the width of the magnetic short-range-order peak certainly does not approach that of a Bragg peak. For the $c = 0.68$ sample, however, it may be possible that a small fraction of the sample manifests long-range order since the top 30% of the main magnetic response has the full width at half maximum of a Bragg peak. This small portion could be associated with the concentration spread noted earlier for this sample (Table I). However, it is clear that the bulk of the sample does not show long-range order. The maximum magnetic cross section observed for all samples is shown as a function of temperature in Fig. 5(b). In each case there is no sign of a sharp increase in intensity which might suggest a phase transition; rather, there is a *gradual* intensity increase as the temperature is decreased with saturation below 10 K. The inverse correlation

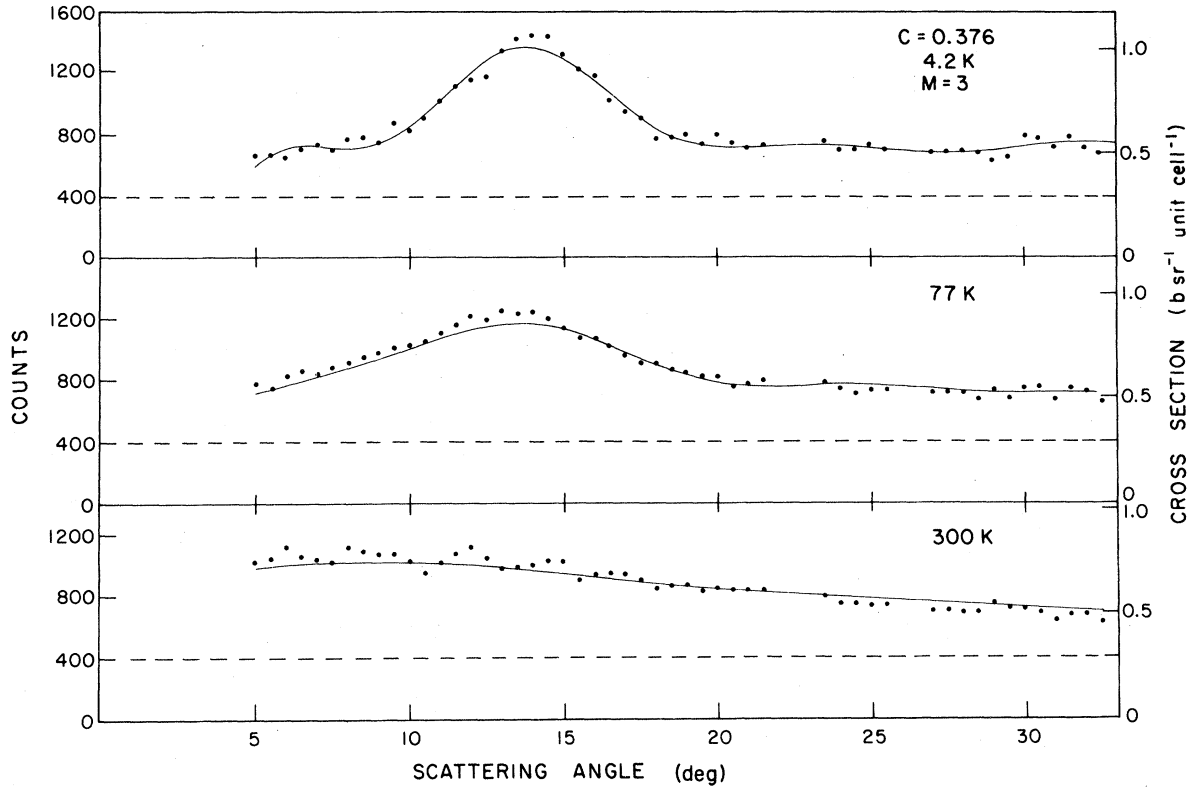

FIG. 2. Temperature dependence of the diffuse neutron scattering from $Mn_{0.376}Zn_{0.624}Te$. The results were corrected for air scattering and for the scattering from the empty sample can and cryostat. The left-hand scale gives the actual observed counts and the right-hand scale gives the cross section obtained by calibration. The dashed line gives the nuclear scattering background obtained from measurements at high angles. The solid lines represent least-squares fits of the theory given in the text to the experimental data. The coherent peaks have been omitted from the figure.

lengths κ_1, assuming that the short-range-order profile is Lorentzian and correcting for a Gaussian resolution, are shown in Fig. 5(a). There is an asymptotic value of κ_1 for each concentration which is reached at about 10 K and which depends strongly on concentration. The composition dependence of the asymptotic value of κ_1 at low temperatures appears to follow a $(c_F-c)^\nu$ dependence with ν between $\frac{1}{2}$ and 1 (Fig. 6), although results at more concentrations are required to obtain the exponent precisely. The conclusion reached is, apart from a caveat for $c=0.68$ mentioned above and because of the possibility of a concentration spread in that sample, that none of the samples actually undergo a phase transition to the ordered state. However, the values of c_F corresponding to the exponent ν are between 0.69 ($\nu=\frac{1}{2}$) and 0.75 ($\nu=1$), indicating that the system is close to a phase transition and this aspect will be explored in future experiments. The appearance of the broad peaks indexing as $(1,\frac{1}{2},0)$ $(1,\frac{3}{2},0)$, and $(2,\frac{1}{2},1)$ suggests that if ordering did occur, it would be type-III antiferromagnetic. This conclusion is strongly supported by the analysis of the results in terms of the theory presented previously.

V. ANALYSIS AND DISCUSSION

The observed variation of magnetic diffuse scattering was fitted to the theory developed previously for correlations between the central spin and successive shells of neighbors as described in Sec. II. The solid curves in Figs. 2–4 represent least-squares fits of the observed scattering to the diffuse and incoherent scattering terms in Eq. (6) with the definition of $g(Q)$ given in Eq. (8). The variable parameters were the Mn spin and the correlations between a central spin and succeeding shells of neighbors on the transition-metal sites, while the nonmagnetic terms were fixed by the scattering at

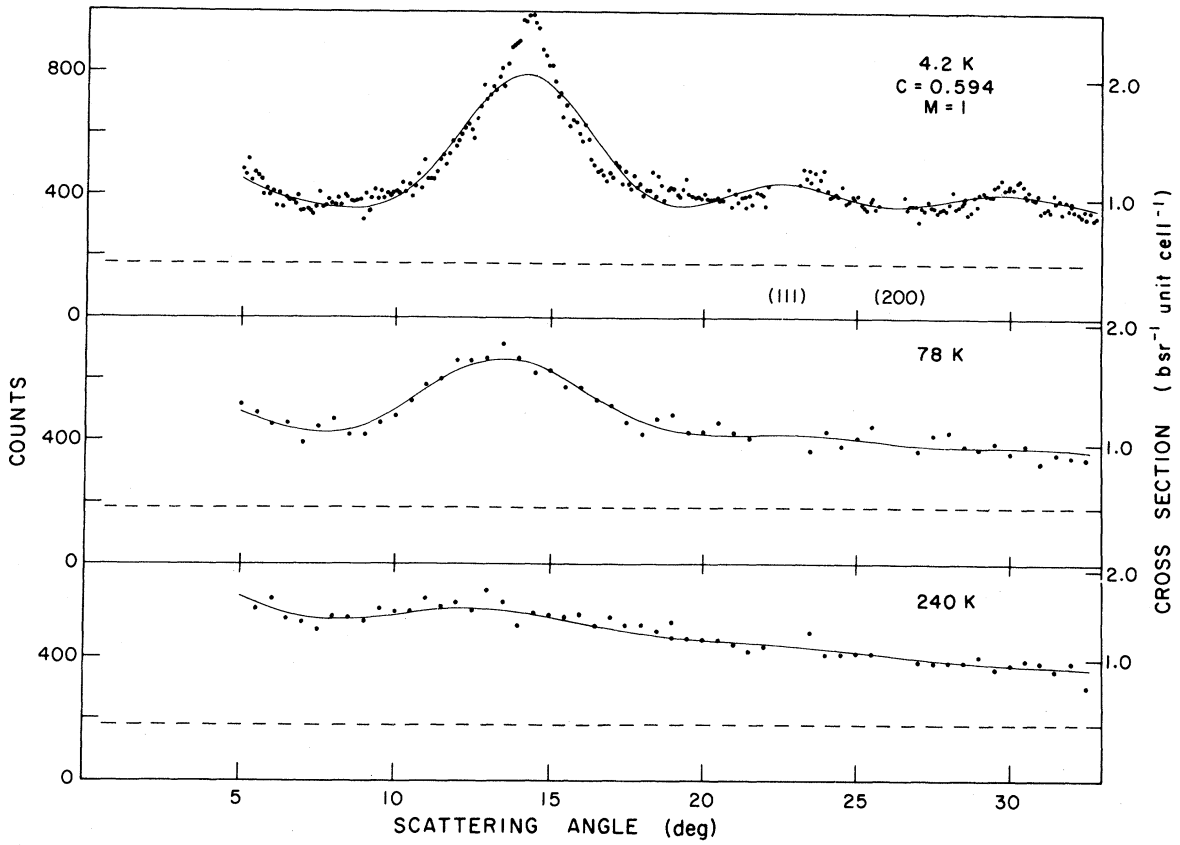

FIG. 3. Temperature dependence of the diffuse neutron scattering from $Mn_{0.594}Zn_{0.406}Te$. Further details are given in the caption of Fig. 1.

high angles where the magnetic scattering is negligible. The results of the fits are collected in Table II for all the temperatures studied. For $c=0.376$ a successful description of the results was obtained over the whole temperature range but the quality of fit was unsatisfactory for the $c=0.594,0.68$ samples below 78 K as can be seen from the corresponding χ values and by inspection of Figs. 2–4. This clearly occurs because the sharpness of the observed diffuse peak cannot be simulated with a limited number of shell terms. If more than seven terms are considered, the errors on the terms derived in the fitting process become comparable with the magnitudes themselves. In the limit where the peaks become sharp, it is possible to use an alternative approach by deriving an inverse correlation length κ_1 (and the radius of gyration, $\langle r_g^2\rangle^{1/2}=\sqrt{3}/\kappa_1$) from the FWHM under the assumption that the line shape is Lorentzian and that the wave-vector resolution is Gaussian.

In spite of the poor quality of fit in some of the cases, the fitted parameters have very reasonable values. They reproduce, for example, the sign sequence of correlations calculated for the perfectly ordered type-III antiferromagnet to seven shells of neighbors, as listed in Table II. The magnitudes of the parameters are also significant. An estimate of the cluster correlations may be made by multiplying the ideal type-III correlations with an envelope function $\exp(-\kappa_1 R_l)$ to limit the spatial range, with κ_1 determined from the $(1,\frac{1}{2},0)$ peak width. These estimates, denoted by filled squares in Fig. 7, are in good agreement with experiment. This result indicates that the correlations are basically such as would occur in perfectly ordered MnTe (if this existed in nature) or β-MnS,[11] but modified so that the correlation decreases exponentially as we move more away from the center of the cluster. The average value of the Mn spin from these experiments is 2.4 ± 0.2, which is consistent with the Hund's-rule value $S=\frac{5}{2}$ for the Mn^{2+} configuration expected in these compounds.

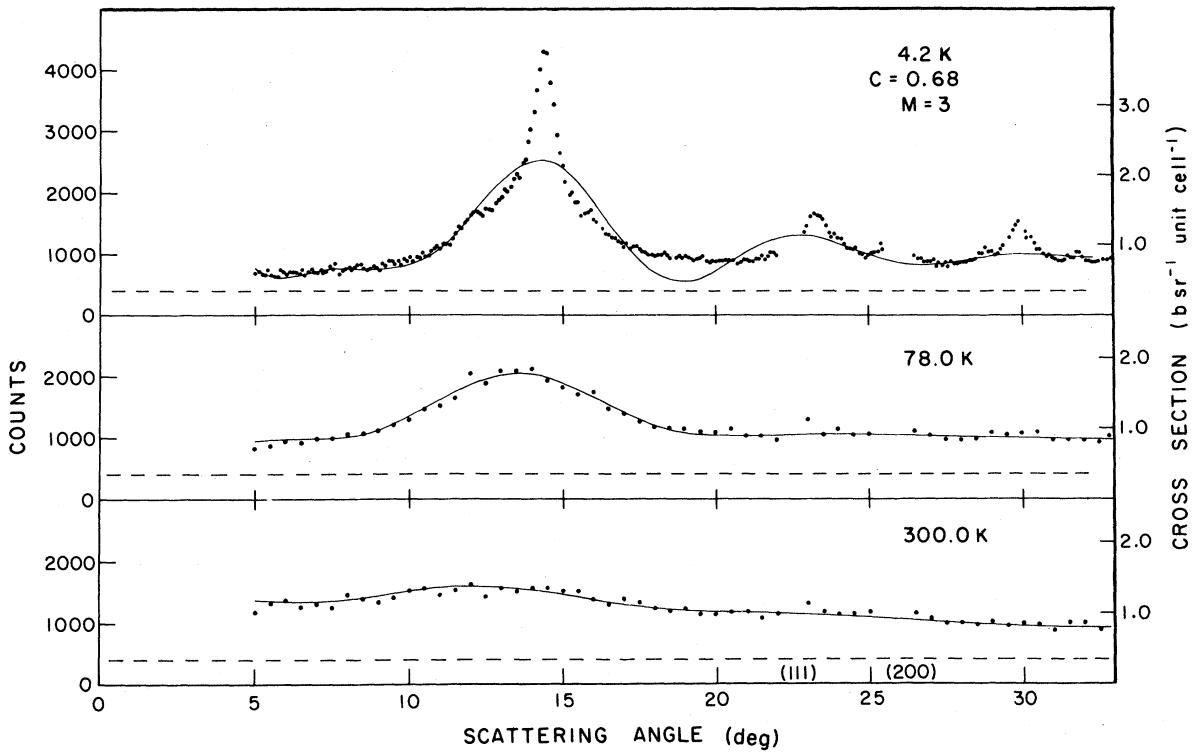

FIG. 4. Temperature dependence of the diffuse neutron scattering from $Mn_{0.676}Zn_{0.423}Te$. Further details are given in the caption of Fig. 1.

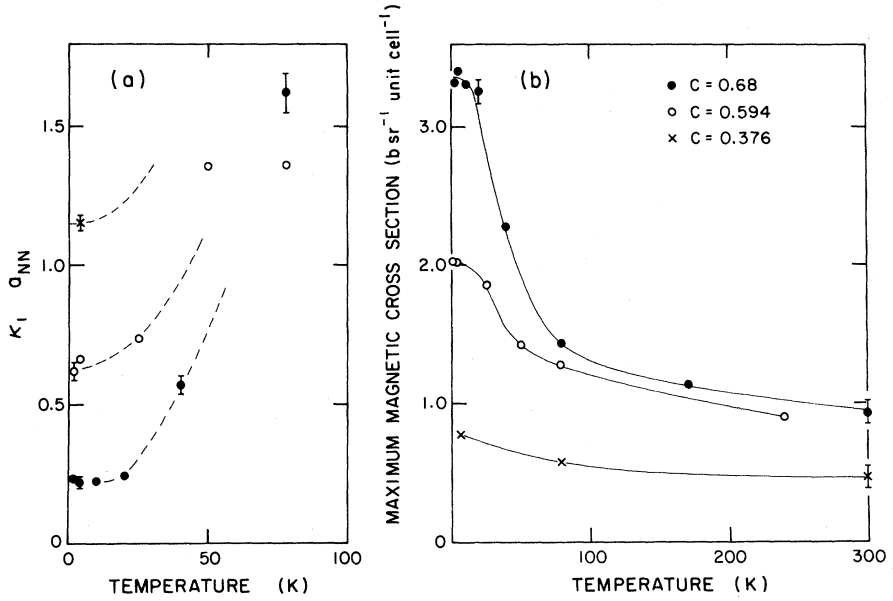

FIG. 5. (a) Temperature dependence of the inverse correlation length for the three samples studied, for those temperatures for which it was possible to measure the FWHM of the magnetic scattering. a_{NN} is the distance between nearest neighbors on the anion sublattice (Table II). (b) Maximum magnetic cross section, obtained from the counts observed in the vicinity of the $(1, \frac{1}{2}, 0)$ magnetic diffuse peak for the three samples studied, as a function of temperature. In each case the intensity increases gradually with decreasing temperature and saturated below 10 K.

TABLE II. Correlations in $Mn_cZn_{1-c}Te$ alloys derived from the magnetic diffuse scattering. A_l-B_l is the sum of the correlations between the central spin and those in the lth coordination shell, A_l^{III} is the sum for an ordered type-III antiferromagnet, S is the Mn^{2+} spin, and χ is the goodness of fit parameter.

c (at. %)	T (K)	A_1-B_1	A_2-B_2	A_3-B_3	A_4-B_4	A_5-B_5	A_6-B_6	A_7-B_7	S	χ
37.6	4.2	−5.6±0.1	1.4±0.2	2.6±0.2	−1.0±0.3	−4.7±0.3			2.20±0.01	1.37
	77	−3.1±0.1	0.3±0.1	2.2±0.2	−1.8±0.2				2.24±0.01	1.31
	300	−0.4±0.1	−0.3±0.1	0.1±0.2					2.19±0.02	1.42
59.4	4.2	−2.2±0.2	1.9±0.2	3.4±0.3	−0.7±0.4	−2.0±0.6	−2.1±0.7	3.8±0.5	2.59±0.02	1.93
	25	−2.5±0.1	1.6±0.1	2.8±0.2	−0.4±0.4	−2.8±0.5	−1.7±0.6	3.0±0.4	2.55±0.01	2.64
	50	−2.6±0.1	1.0±0.1	1.5±0.1	−0.2±0.2	−2.2±0.3	−0.8±0.3	0.5±0.2	2.54±0.01	1.50
	78	−1.6±0.1	0.7±0.1	1.7±0.2	−0.1±0.2	−0.1±0.2			2.59±0.01	1.09
	240	−0.1±0.1	0.3±0.1	0.7±0.1					2.56±0.01	1.03
68.0	4.2	−2.3±0.3	1.3±0.3	6.1±0.5	−1.3±0.8	−3.4±1.1	−1.4±1.1	6.3±0.8	2.40±0.03	6.93
	40	−2.7±0.1	1.5±0.1	3.4±0.2	−0.7±0.4	−2.5±0.5	−0.6±0.6	2.6±0.4	2.45±0.01	3.28
	78	−2.3±0.1	0.6±0.1	2.1±0.1	−1.3±0.2	−0.1±0.3	−1.0±0.3	0.5±0.2	2.49±0.01	1.93
	170	−1.1±0.1	−0.1±0.1	1.6±0.1	−0.6±0.1				2.50±0.01	1.53
	300	−0.5±0.1	−0.1±0.1	0.7±0.1					2.43±0.01	1.14
A_l^{III}		−4	+2	+16	−8	−8	−8	+16		
l		$\sqrt{2}a/2$ (4.4 Å)	a (6.2 Å)	$\sqrt{6}a/2$ (7.6 Å)	$\sqrt{2}a$ (8.8 Å)	$\sqrt{10}a/2$ (9.8 Å)	$\sqrt{3}a$ (10.7 Å)	$\sqrt{14}a/2$ (11.6 Å)		

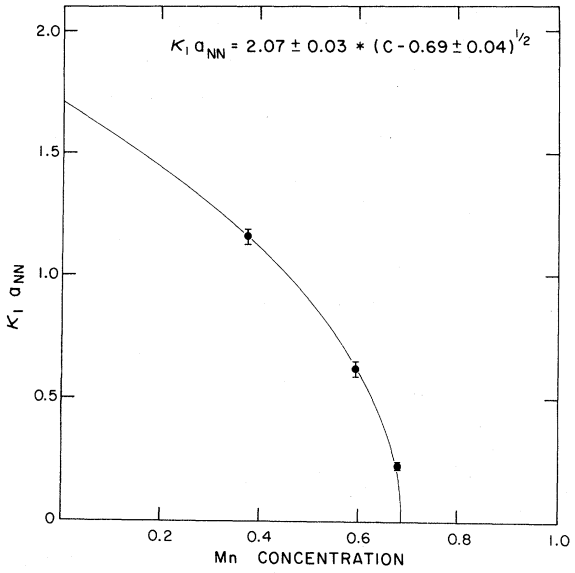

FIG. 6. Concentration dependence of the low-temperature asymptotic value of the inverse correlation length. The solid curve is the best fit to a $(c_F - c)^{\nu}$ dependence of the inverse correlation length on concentration with $\nu = \frac{1}{2}$. The fit suggests that the critical concentration for magnetic ordering lies just above the maximum concentration studied.

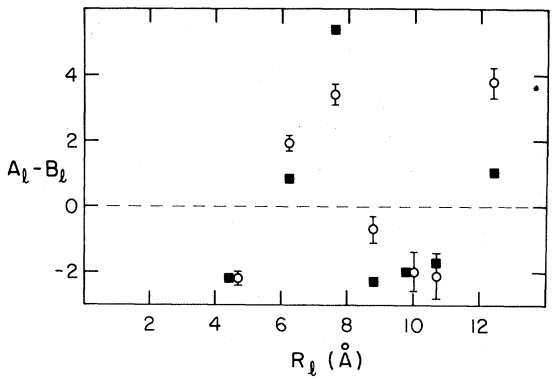

FIG. 7. Comparison of the fitted correlation parameters $(A_l - B_l)$ between the central spin and successive shells of neighbors for $c = 0.594$ at 4.2 K and the correlation parameters for an ordered type-III antiferromagnet as modified by an exponential envelope $\exp(-\kappa_1 R_l)$. κ_1 was determined from the width at half-height of the $(1, \frac{1}{2}, 0)$ magnetic diffuse peak at 4.2 K and was corrected for the finite wave-vector resolution.

The present results are very similar to those for quenched CuMn alloys.[5] The first- and second-neighbor correlations are antiferromagnetic and ferromagnetic, respectively, like $Mn_cMn_{1-c}Te$. At concentrations below the antiferromagnetic transition in CuMn which occurs at 72 at.% Mn, the correlations grow in magnitude and range as the temperature is decreased, with saturation below 100 K. Quenched CuMn alloys exhibit spin-glass behavior (a cusp in the static susceptibility) and so does $Mn_cZn_{1-c}Te$ (Ref. 16) and the sister alloys $Mn_cCd_{1-c}Te$ (Ref. 3) and $Mn_cHg_{1-c}Te$ (Ref. 2). As stressed earlier, there is only evidence for the gradual growth of correlations with temperature and no temperature can be singled out to represent the freezing temperature from the neutron diffraction measurements. However, there are also significant differences between CuMn and $Mn_cZn_{1-c}Te$ since the fluctuations found near $(1, \frac{1}{2}, 0)$ in CuMn are not precursors to type-III antiferromagnetism; the eventual magnetic structure[17] is type-I antiferromagnetic in a face-centered tetragonal lattice with ordering wave vector (110). Single-crystal studies[6] suggest to us that the magnetic short-range order, which peaks at $(1, \frac{1}{2} \pm \delta, 0)$ is fundamentally driven by the nuclear short-range order. That is, the correlations in $Mn_cZn_{1-c}Te$ arise because the exchange favors type-III antiferromagnetism, whereas in CuMn they arise partly because Mn ions prefer to have more copper than manganese ions as nearest neighbors below 60% (in an arrangement that is the chemical analog of the type-III structure with Cu neighbors standing for antiparallel spins) and more manganese than copper neighbors above that concentration.

The behavior of the inverse correlation length κ_1 in Fig. 5(a) is analogous to the behavior of κ_1, for CrFe (Ref. 18) alloys and several transition-metal fluorides[19] with mixtures of nonmagnetic and magnetic ions on the transition-metal sites close to, but below, the percolation concentration. The inverse correlation length saturated at low temperatures and was also shown[19] to be the sum of a geometrical and a thermal part that vanishes at 0 K. The best theoretical estimate[20] of the exponent ν in the power-law dependence $(c_F - c)^{\nu}$ is 0.845 ± 0.021. Further experiments to determine the precise thermal and geometrical exponents are planned.

ACKNOWLEDGMENTS

We are grateful to H. F. Nieman, M. M. Potter, D. C. Tennant, A. H. Hewitt, and J. C. Evans for providing valuable technical assistance. One of us (J.K.F.) gratefully acknowledges the support of the National Science Foundation Grants Nos. DMR79-23310 and DMR80-20249.

[1]J. A. Gaj, in Proceedings of the International Conference on the Physics of Semiconductors, Kyoto, Japan, 1980 [J. Phys. Soc. Jpn. 49, 1071 (1980)].

[2]R. R. Galazka, S. Nagata, and P. H. Keesom, Phys. Rev. B 22, 3344 (1980).

[3]S. Nagata, R. R. Galazka, D. P. Mullin, H. Akbarzadeh, G. D. Khattak, J. K. Furdyna, and P. H. Keesom, Phys. Rev. B 22, 3331 (1980).

[4]P. Wells and J. H. Smith, J. Phys. F 1, 763 (1971).

[5]J. R. Davis, S. K. Burke, and B. D. Rainford, J. Magn. Magn. Mater. 15-18, 151 (1980).

[6]S. A. Werner and J. W. Cable, J. Appl. Phys. 52, 1757 (1980).

[7]A. P. Murani, S. Roth, R. Radhakrishna, B. D. Rainford, B. R. Coles, K. Ibel, G. Goeltz, and F. Mezei, J. Phys. F 6, 425 (1976); A. P. Murani, Phys. Rev. Lett. 37, 450 (1976).

[8]H. Maletta and W. Felsch, Z. Phys. B 37, 55 (1980).

[9]W. Nagele, K. Knorr, W. Prandl, P. Convert, and J. L. Buevoz, J. Phys. C 11, 3295 (1978).

[10]A. Pajaczkowska, Prog. Cryst. Growth Charact. 1, 289 (1978).

[11]L. Corliss, N. Elliott, and J. N. Hastings, Phys. Rev. 104, 924 (1956).

[12]J. S. Smart, *Effective Field Theories of Magnetism* (Saunders, Philadelphia, 1966).

[13]W. Marshall and S. W. Lovesey, *Theory of Thermal Neutron Scattering* (Clarendon, Oxford, 1971).

[14]V. F. Sears, Adv. Phys. 24, 1 (1975); Nucl. Instrum. Methods 123, 521 (1975).

[15]L. Koester, *Neutron Physics,* Vol. 80 of *Springer Tracts in Modern Physics* (Springer, Berlin, 1977).

[16]J. K. Furdyna and S. McAlister (private communication).

[17]D. Meneghetti and S. S. Sidhu, Phys. Rev. 105, 130 (1957).

[18]B. D. Rainford, S. K. Burke, J. R. Davis, and W. Howarth, in Proceedings of the Symposium on Neutron Scattering, Argonne National Laboratory, 1981 (AIP, New York, in press).

[19]R. A. Cowley, Philos. Trans. R. Soc. London Ser. B 290, 583 (1980).

[20]S. Kirkpatrick, in *Electrical Transport and Optical Properties of Inhomogeneous Media (Ohio State University, 1977),* Proceedings of the First Conference on the Electrical Transport and Optical Properties of Inhomogeneous Media, edited by J. C. Garland and D. B. Tanner (AIP, New York, 1978).